AFRL-RV-PS-
TR-2018-0118

UNDERSTANDING MECHANISMS OF RADIATION DEGRADATION IN ELECTRONIC AND OPTOELECTRONIC DEVICES: A MULTI-TIMESCALE MODEL

Fei Gao

Regents of the University of Michigan
Office of Research and Sponsored Projects
503 Thompson Street
Ann Arbor, MI 48109-1340

16 October 2018

Final Report

AIR FORCE RESEARCH LABORATORY
Space Vehicles Directorate
3550 Aberdeen Ave SE
AIR FORCE MATERIEL COMMAND
KIRTLAND AIR FORCE BASE, NM 87117-5776

DTIC COPY

NOTICE AND SIGNATURE PAGE

This report is the result of contracted fundamental research which is exempt from public affairs security and policy review in accordance with AFI 61-201, paragraph 2.3.5.1. This report is available to the general public, including foreign nationals. Copies may be obtained from the Defense Technical Information Center (DTIC) (http://www.dtic.mil).

AFRL-RV-PS-TR-2018-0118 HAS BEEN REVIEWED AND IS APPROVED FOR PUBLICATION IN ACCORDANCE WITH ASSIGNED DISTRIBUTION STATEMENT.

//signed//	//signed//
DAVID CARDIMONA	JOHN BEAUCHEMIN
Program Manager/Tech Advisor	Chief Engineer, Spacecraft Technology Division
Missile Warning & ISR Technology Branch	Space Vehicles Directorate

REPORT DOCUMENTATION PAGE

Form Approved
OMB No. 0704-0188

1. REPORT DATE *(DD-MM-YYYY)*
16-10-2018

2. REPORT TYPE
Final Report

3. DATES COVERED *(From - To)*
17 Oct 2016 – 17 Oct 2018

4. TITLE AND SUBTITLE
Understanding Mechanisms of Radiation Degradation in Electronic and Optoelectronic Devices: A Multi-timescale Model

5a. CONTRACT NUMBER

5b. GRANT NUMBER
FA9453-17-2-0010

5c. PROGRAM ELEMENT NUMBER
62601F

6. AUTHOR(S)
Fei Gao

5d. PROJECT NUMBER
4846

5e. TASK NUMBER
PPM00035612

5f. WORK UNIT NUMBER
EF129429

7. PERFORMING ORGANIZATION NAME(S) AND ADDRESS(ES)
AND ADDRESS(ES)
Regents of the University of Michigan
Office of Research and Sponsored Projects
503 Thompson Street
Ann Arbor, MI 48109-1340

8. PERFORMING ORGANIZATION REPORT NUMBER

9. SPONSORING / MONITORING AGENCY NAME(S) AND ADDRESS(ES)
Air Force Research Laboratory
Space Vehicles Directorate
3550 Aberdeen Ave., SE
Kirtland AFB, NM 87117-5776

10. SPONSOR/MONITOR'S ACRONYM(S)
AFRL/RVSU

11. SPONSOR/MONITOR'S REPORT NUMBER(S)
AFRL-RV-PS-TR-2018-0118

12. DISTRIBUTION / AVAILABILITY STATEMENT
Approved for public release; distribution is unlimited.

13. SUPPLEMENTARY NOTES

14. ABSTRACT

The purpose of this funding is to support the development of a theory to describe effects of radiation-induced defects in electronic and optoelectronic devices. No actual experiments will be performed on this effort. This project will continue a research effort at the University of Michigan to simulate atomistic, and meso-scale behavior of defect evolutions in compound semiconductors, including ultrafast displacement cascade, intermediate defect stabilization and cluster formation, as well as slow defect reaction and migration. Based on atomic-level simulations, non-ionization energy loss has been determined.

15. SUBJECT TERMS

Non-ionizing Energy Loss, NIEL, Defect Generation, Radiation Degradation, Semiconductors, Ultrafast Displacement Cascade, GaAs, GaN

16. SECURITY CLASSIFICATION OF:			**17. LIMITATION OF ABSTRACT**	**18. NUMBER OF PAGES**	**19a. NAME OF RESPONSIBLE PERSON** Dave Cardimona
a. REPORT Unclassified	**b. ABSTRACT** Unclassified	**c. THIS PAGE** Unclassified	Unlimited	38	**19b. TELEPHONE NUMBER** *(include area code)*

Standard Form 298 (Rev. 8-98)
Prescribed by ANSI Std. 239.18

(This page intentionally left blank)

TABLE OF CONTENTS

LIST OF FIGURES

1. SUMMARY

This project continues a research effort at the University of Michigan to simulate atomistic- and meso-scale behavior of defect evolutions in compound semiconductors, including ultrafast displacement cascades, intermediate defect stabilization, and cluster formation, as well as slow defect reaction and migration. The fundamental mechanisms and knowledge gained from atomic- and meso-scale simulations will be input into rate-diffusion theory as initial conditions to calculate the steady-state distribution of point defects in a mesoscopic layered-structured system, thus allowing the development of a multi-timescale theory to study radiation degradation in electronic and optoelectronic devices. To achieve this goal, we have further analyzed the results from molecular dynamics simulations and compared the defect production, defect morphology, and defect clustering in GaAs and GaN, as well as the non-ionizing energy loss (NIEL), a model developed based on atomic-level information in previous fiscal year. In general, the calculated NIEL in GaN is often found smaller than that predicted by a model based on the simple Kinchin-Pease formula or SRIM calculations. The comparisons of defect creation, density, and effective NIEL in GaN to those of GaAs suggest that GaN may be much more resistant to displacement damage than GaAs, and therefore, very suitable for use in high-power space-energy systems and space-probe applications. Based on an analytical bond-order potential (ABOP) approach, we have developed the interatomic potentials for indium arsenide (InAs), but the detailed calculations demonstrate that the potentials are not good enough for describing the properties of all possible defects in InAs. Thus, we have launched a comprehensive study of the formation and electronic structures of 15 kinds of intrinsic point defects in InAs using first-principles calculations. The substitutional point defects are the primary intrinsic point defects except the shallow doped In-rich environment where the dominant intrinsic point defects are In tetrahedral interstitials. The dumbbell interstitials prefer <110> configurations. For tetrahedral interstitials, In atoms prefer a 4-As tetrahedral site under both As-rich and In-rich environments. The most popular vacancy-type defect is V_{In} (vacancy on In site) in As-rich environment, but switched to V_{As} (vacancy on As site) in In-rich environment. These defect properties are used to refit the interatomic potentials for InAs, which should be suitable for simulating defect generation. The simulations of defect generation and defect clustering and the calculations of the effect of NIEL in InAs are in progress. In addition, one journal paper and one conference paper that compare the simulation results of GaN and GaAs have been published, and another paper describing *ab initio* calculations of defect properties in InAs is prepared for submission.

2. INTRODUCTION

Semiconductor compounds from the III-V direct band gap family have received considerable attention and been extensively studied for the last decades due to some unique properties. For example, those semiconductors often exhibit a large band gap, strong interatomic bonds, and a high thermal conductivity, which make them ideal materials for optoelectronic and high-temperature/high-power devices. Their applications have also been extended to the replacement of silicon in microelectronic components [1, 2] and solar cells [3]. In compound semiconductors, GaN, GaAs and InAs have been proposed to be used for high-power space-energy systems and space-probe applications, including those for satellites or avionics with radiation hardness being a key requirement [4,5]. However, for space-based applications, electronic devices are often exposed to high fluxes of cosmic rays including protons, α-particles, and other heavier ions. These high-energy charged particles would cause space radiation damage, which may degrade the electrical performance of many devices, being a limiting factor to GaN, GaAs and InAs on interplanetary missions unless sufficient shielding is provided to keep damage levels under acceptable limits. A variety of experimental techniques has been used to study the effect of radiation in compound semiconductors. Meanwhile, as a means of fabricating optoelectronic devices, the well-known technique of ion implantation is often used on an industrial scale. Thus, the interaction of atoms of compound semiconductors with highly energetic ions could inevitably result in point defects, defect clusters, and even disordering. A full understanding of defect production, stabilization, clustering, migration, and interaction with microstructural imperfection in compound semiconductors is a crucial aspect for developing a multiscale theory to explore radiation degradation in electronic and optoelectronic devices.

Ab initio calculations based on density functional theory (DFT) are employed to determine defect properties, while a large scale molecular dynamics method is used to simulate displacement damage and defect generation. One of the fundamental questions is the formation energy of the point defects, which is required to understand the creation of defects from an energetics aspect. In addition, thermodynamic arguments suggest that the intrinsic or native defects will be inevitably present within a crystal under finite temperatures or under irradiation. Therefore, *ab initio* calculations of the formation energy of various point defects will provide insights to understand defect energetics within the bulk crystals. Generally, DFT describes reasonably well the structural properties, such as lattice constants and bulk moduli [6]. The aims of *ab initio* studies of defect properties are to provide an extensive and accurate study on the intrinsic point defect formation which is missed in the literature, for example a very recent computational study [7], but desirable. In addition, these calculations will provide important inputs for fitting interatomic potentials for large scale molecular dynamics simulations of displacement damage.

As described in our previous reports, we have developed a model for studying non-ionizing energy loss (NIEL) in compound semiconductors, which is based on atomic-level simulation of radiation damage, and the model has been applied to study GaAs [8] and GaN [9]. NIEL is a calculation of the rate of energy loss due to atomic displacements as an incoming particle traverses a material, and the product of the NIEL and the particle fluence gives the displacement damage energy along the track. Many studies have successfully demonstrated that the degradation of semiconductor devices or optical sensors in a radiation field can be linearly correlated to the displacement damage energy, and subsequently to the NIEL deposited in the semiconductor devices or optical sensors [10-12]. Understanding these correlations is of importance for space applications since the space environment consists of high energy particles. The energies of some particles are high enough to penetrate hard satellite shielding material and interact with the sensitive internal sensors, often made of semiconducting materials. Therefore, understanding radiation damage mechanisms in GaAs and GaN as described by the NIEL model is essential in the development and design of electronics for space applications.

We present a detailed molecular dynamics (MD) study of defect generation, defect clustering, and disordering of GaN and GaAs. Specifically, the displacement cascades were studied in a wide energy range (0.5-20 keV). Effective NIELs in both GaN and GaAs after incident particle impact (i.e. proton, α, and Xe) were compared in combination with the knowledge acquired by atomic simulations and energy partition functions. In addition, we present an *ab initio* approach to determine defect formation energy and the corrections, and the computational details of DFT calculations for InAs. The results and analysis of formation energy of the fifteen intrinsic defects in five groups as a function of Fermi level under different chemical environments and charge states is provided, based on which the new interatomic potentials are developed.

3. METHODS, ASSUMPTIONS, AND PROCEDURES

3.1. MD Simulation of Effective NIEL

The MD method has been employed to perform the defect generation process. All of the MD simulations were performed using an updated version of the code MOLDY [13], which has been modified to semiconductors [8,9]. Constant volume and constant number of atoms were applied to each simulation with periodic boundary conditions in three directions. MD cell size was carefully chosen for different cases to avoid the overlap of a displacement cascade with itself due to periodicity. For a displacement cascade of 20 keV, a crystal of 1000000 atoms (50×50×50 unit cells) is employed for simulation. The lattice temperature is initially set to 100 K, which imitates a thermal energy just about zero-point value. During the simulation, the computational block was held at a temperature of 100 K and equilibrated for 10 ps prior to a recoil event to achieve an equilibrium phonon state. A single cascade was simulated by given a gallium primary recoil atom (Ga-PKA) a kinetic energy equal to the damage energy, and the subsequent evolution was followed for 20 ps. We have carried out simulations of displacement cascades in the energy range from 500 eV to 20 keV, and at least 20 PKA events were performed at each energy in various crystallographic directions to maintain a good statistic. Interstitials and vacancies were recognized in the simulations using a Wigner-Seitz cell analysis of the atom positions.

The interactions between atoms were described by analytical bond-order potentials developed for GaN [14] and GaAs [15], respectively. These potentials have been widely used to study a variety of properties of GaN and GaAs. The excellent description of their properties as compared with the experimental data and first-principle calculations validates its accuracy and transferability of the potentials. However, it still has its shortage in obtaining a satisfactory description in the short-range interactions which are important to simulate atomic displacement and defect creation at high recoil energies. To overcome this deficiency, the potential has been further modified by adding a repulsive potential, Ziegler-Biersack-Littmark (ZBL) ‘Universal’ potential [16], which optimally describes the high energy scattering of atoms in solids. This is achieved by coupling the original BOPs and the short-range function through the use of Fermi-type function.

$$F(r) = \frac{1}{1 + e^{-b_f(r-r_f)}}, \tag{1}$$

where $F(r)$ quickly goes to one as r increases. The total potential is given by connecting BOP to ZBL potential,

$$F(r) = V_{ZBL}[1 - F(r)] + V_{BOP}F(r), \tag{2}$$

which yields a repulsive potential that is dominated by the ZBL for a very short distance and quickly approaches the BOP as *r* increases, as desired. The parameters of b_f and r_f are adjusted to make sure that the potential and its first derivative are smoothly transitioned. The values of bf are determined to be 14, 14, and 7.5 Å^{-1} for both of GaN and GaAs system. The values r_f that has been used for Ga-Ga, Ga-N, and N-N interactions are 0.86, 0.95 and 0.60 Å, respectively, while the values used for Ga-Ga, Ga-As, and As-As are 0.95, 0.95, and 0.65 A, respectively.

Conventionally, the NIEL can be determined through Linhard energy partition function, G(T) [17]

$$NIEL = \alpha \int_{E_d}^{T_{max}} T \frac{d\delta}{dT} G(T) dT, \tag{3}$$

where α is the atomic density of the target material, T the kinetic energy of the recoil, T_{max} the maximum energy that can be transferred to a recoil nucleus by an incident particle. $E_d$stands for the threshold displacement energy. At low incident energies, the NIEL is sensitive to the values of the threshold energy used. As is already known, unlike SiC, the E_d of GaAs is weakly depends on the crystallographic direction [18]. It is taken to be 25 eV conventionally. However, GaN finds an average threshold displacement energy in all directions to be 50 eV, which is in excellent agreement with available experimental data. $\frac{d\delta}{dT}$ is the differential interaction cross section. At low energy, the recoil energy of a PKA, E_{PKA}, is close to T, but at high energy most of the energy of a PKA contributes to ionization. Since the number of displacements can be estimated through $G(T)$ by the Kinchin-Pease (K-P) model, it can be rewritten by

$$NIEL = \alpha \int_{E_d}^{T_{max}} F(T) G(T) \frac{d\delta}{dT} dT, \tag{4}$$

where $(T) = \frac{E_d}{0.4} N_F(T)$. Based on K-P model, it has long been realized that N_F is proportional to the recoil energy, showing a linear relation between NIEL and the number of defects produced by irradiation. However, the NIEL is not necessarily proportional to N_F, due to non-linear process happened in semiconductor. Accordingly, based on MD simulations, we introduce an "effective NIEL" where the non-linear features are taken in to account

$$NIEL = \alpha \int_{E_d}^{T_{max}} \frac{E_d}{0.4} N_F^{MD} G(T) \frac{d\delta}{dT} dT, \tag{5}$$

Thus, $N_F^{MD}(T)$ results from the MD simulation being the number of defects produced at a given recoil energy of T. The ZBL Universal Formalism is chosen to calculate the differential interaction cross section [19],

$$\frac{d\delta}{dT} = -\frac{\pi a_U^2 f(t^{1/2})}{2t^{3/2}}, \tag{6}$$

where $t = \epsilon^2 T / T_{max}$ is a dimensionless collision parameter related to recoil energy T, ϵ is the ZBL reduced energy, and a_U is the ZBL Universal screening length. $f(t^{1/2})$ refers to Thomas-Fermi scattering function [19,20]. The energy partition function used throughout the study is described as

$$G(T) = -\frac{1}{1 + k_d g(\epsilon_d)}, \tag{7}$$

where k_d, ϵ_d, and $g(\epsilon_d)$ are dimensionless parameters, and their detailed formulas and values are described elsewhere [19].

3.2. AB Initio Calculation Method

Ab initio calculation was applied to investigation of intrinsic defects of InAs. The conventional unit cell contains eight atoms (four indium and four arsenic atoms). We used a 3 × 3 × 3 supercell containing 216 regular lattice sites, which consists of 108 indium and 108 arsenic atoms before introduction of defects. The total energies of the system and forces on each atom are characterized via first-principles calculations within the framework of DFT. All DFT calculations were carried out with the Vienna Ab-initio Simulation Package (VASP) [21,22] which is based on the Kohn-Sham Density Functional Theory (KS-DFT) [23,24] with the generalized gradient approximations of the exchange-correlation functions [25] as parameterized by Perdew, Burke and Ernzerh (PBE) revised for solids (PBEsol) [26]. The electrons explicitly included in the calculations are the 5s25p1 and 4s24p3 electrons for indium and arsenic atoms, respectively. The core electrons are replaced by the projector augmented wave (PAW) and pseudo-potential approach [43, 44]. A plane-wave cutoff of 400 eV is used in the geometry relaxation to reduce Pulay stress. For all other calculations, we used a plane-wave cutoff of 400 eV with accurate and dense k-mesh. The irreducible Brillouin Zone was sampled with a Gamma-centered 3 × 3 × 3 k-mesh for all the calculations. The calculations are performed at zero temperature. The criterion to stop the relaxation of the electronic degrees of freedom is set by total energy change to be smaller than 10^{-5} eV. The optimized atomic geometry was achieved through minimizing Hellmann-Feynman forces acting on each atom until the maximum forces on the ions were smaller than 0.01 eV/Å.

After geometry optimization of the perfect crystal, we introduced defects by either removal of an appropriate atom to create a vacancy, or addition of an extra atom to create an interstitial in a pre-specified position (tetrahedral or dumbbells). The resulting structures are allowed to relax energetically, permitting atoms to move in all three dimensions. Geometry optimization is performed using the classical conjugate gradient algorithm.

4. RESULTS AND DISCUSSION

4.1. Effective NIEL: A Comparative Study of GaN and GaAs

4.1.1. Cascade Morphology

The approach of MD simulations and the atomic-level based NIEL model have been detailed in [8] and previous reports. Here, we only summarize the main results obtained from the simulations.

Similar to other semiconductors, the displacement cascades modeled in the present work exhibit two basic phases, i.e., a ballistic phase and a recombination phase. The ballistic phase can live for a few tenths of picoseconds, during which a rapid build-up in the number of displaced atoms is established. Displacement damage occurs when sufficient energy is transferred from an incident energetic particle to a lattice atom to dislodge it from its normal location. The number of displacements increases with time, reaching a maximum amount (known as peak damage state) at around 1 ps. Subsequently, the system cools down and the recombination process occurs.

A typical 10 keV cascade of GaAs and GaN at their peak and final damage states are shown in Figure 1 (a) and (b), and Figure 1 (c) and (d), respectively. Only displaced atoms and antisite defects are demonstrated for better view. The interstitials are represented by large spheres and vacancies by small ones. Every lattice site is associated with a regime defined by a Wigner-Seitz cell. The vacancies are lattice sites that have no atoms within a Wigner-Seitz cell, while two or more atoms within a cell indicates interstitials. At 10 keV, the cascades in GaAs are clearly broken up into spatially separated subcascades as shown in Figure 1 (a), which is similar to the observation for Si [27]. These subcascades form distinct regions, in which a number of atoms are displaced. The primary knock-on atom (PKA) in GaN results in a lot of displacements at peak damage and the defect density within the cascade region is high (see Figure 1 (c)), which lead to a sharp thermal spike. This feature is unique in comparison with those in GaAs and SiC. At final damage state, the remaining number of displaced atoms in GaAs as illustrated in Figure 1 (b) is surprisingly comparable to those at peak damage state with only 20% recombination with vacancies, which means the recombination in GaAs is mild. This phenomenon can be explained by the low threshold displacement energy of GaAs [18] as the PKA is able to create disordered regions, leading to the formation of amorphous domains, which eventually prevent the displaced atoms from recombining with the empty lattice sites. In contrast to the displacement cascade in GaAs, the recombination of displacement atoms with vacancies is significant in GaN due to the pseudo-metallic behavior (PMB). The recombination level reaches 96% as compared with that in a real metal [28] and SiC [29], where a typical cascade leads to a recombination of 90% and 50% of displacement atoms with empty lattice sites, respectively. Direct inspection of the defects (Figure 1 (d)) indicates the majority of surviving defects are just single interstitials or vacancies associated with a small amount of clusters. In order to further characterize the evolution and nature of these cascades, the number of antisite defects and atoms displaced into interstitial positions from both GaAs and GaN are plotted in Figure 2 (a) and Figure 2 (b) as a function of time for a 10 keV and 20 keV cascade, respectively. Within a certain time range from beginning to peak damage at t_{peak} 0.5 ps, the number of displaced atoms, N_d, increases with the increasing of time. Beyond this range, the N_d decreases as recombination processes take place. It is of interest to note that the number of "interstitial" defects declines rapidly to final values within 1.2 ps and 3 ps for GaAs and GaN, respectively.

This demonstrates that the cascade lifetime, defined as the time during which the number of defects reaches its final value, is very short for both GaAs and GaN, similar to SiC [29,30]. As aforementioned, the recombination is not significant in GaAs. Only a slight decrease has been illustrated in Figure 2. Most antisite defects in GaAs are generated during the collisional phase, and the increase in antisite defects is very small during relaxation, where multiple amorphous domains prevent them from recovery. Unlike GaAs, the surviving defects generated in the primary damage indicate that the direct-impact amorphization in GaN does not exist during the cascade lifetime. Additionally, the antisite defects can be easily recovered. This gives evidence that the formation of antisite defects in GaN might result from the short replacement collision sequences.

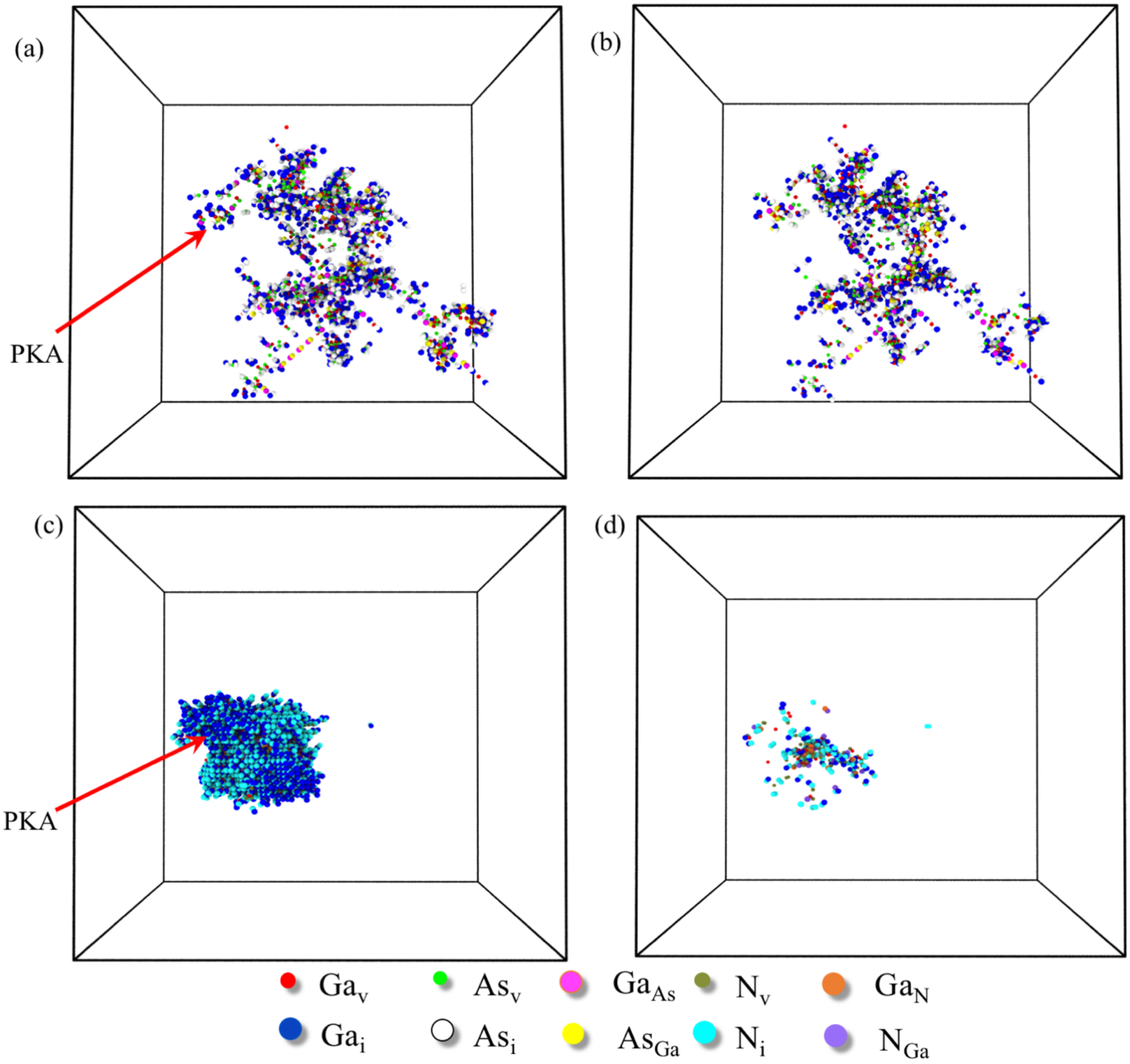

Figure 1. A Typical 10keV Cascade in (a) GaAs at Peak Damage (b) GaAs at Final Damage (c) GaN at Peak Damage (d) GaN at Final Damage

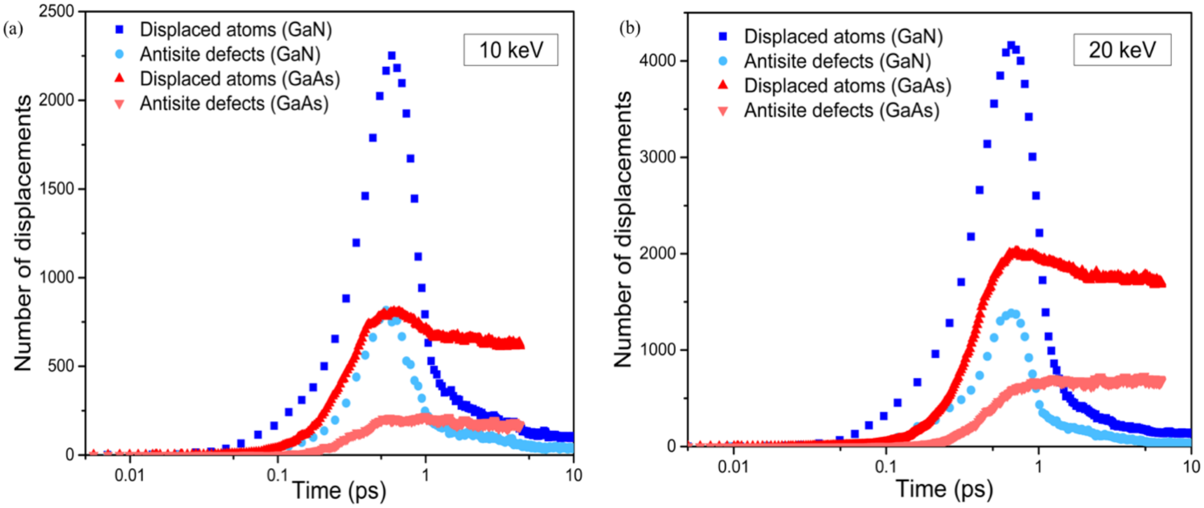

Figure 2. Comparison of GaN and GaAs in Terms of Number of Displacements and Anti-site defects at (a) 10 keV and (b) 20 keV

Figure 3 presents cascade morphology of GaAs and GaN at the final defect state ranging from 2 to 20 keV. On the one hand, multiple sub-branches of a cascade along the collision path were observed in GaAs for all energy cases, forming amorphous domains. It is highly likely that the defects generated by a PKA energy under 2 keV exist only within a single-cascade region. The sub-cascade feature becomes more evident as shown in Figure 3 (b) and Figure 3 (c), which suggests that nonlinear effects take place in higher energy (>2 keV) cascades. On the other hand, the cascade morphology of GaN is not the same as GaAs. For all the energies considered, sub-branches of cascades are invisible, while a single-cascade region is verified by Figure 3 (d)-(f). The surviving defects within the single-cascade region are mainly single interstitials and mono-vacancies with a small portion of defect clusters which is consistent with the observation in the 10 keV cascade discussed earlier.

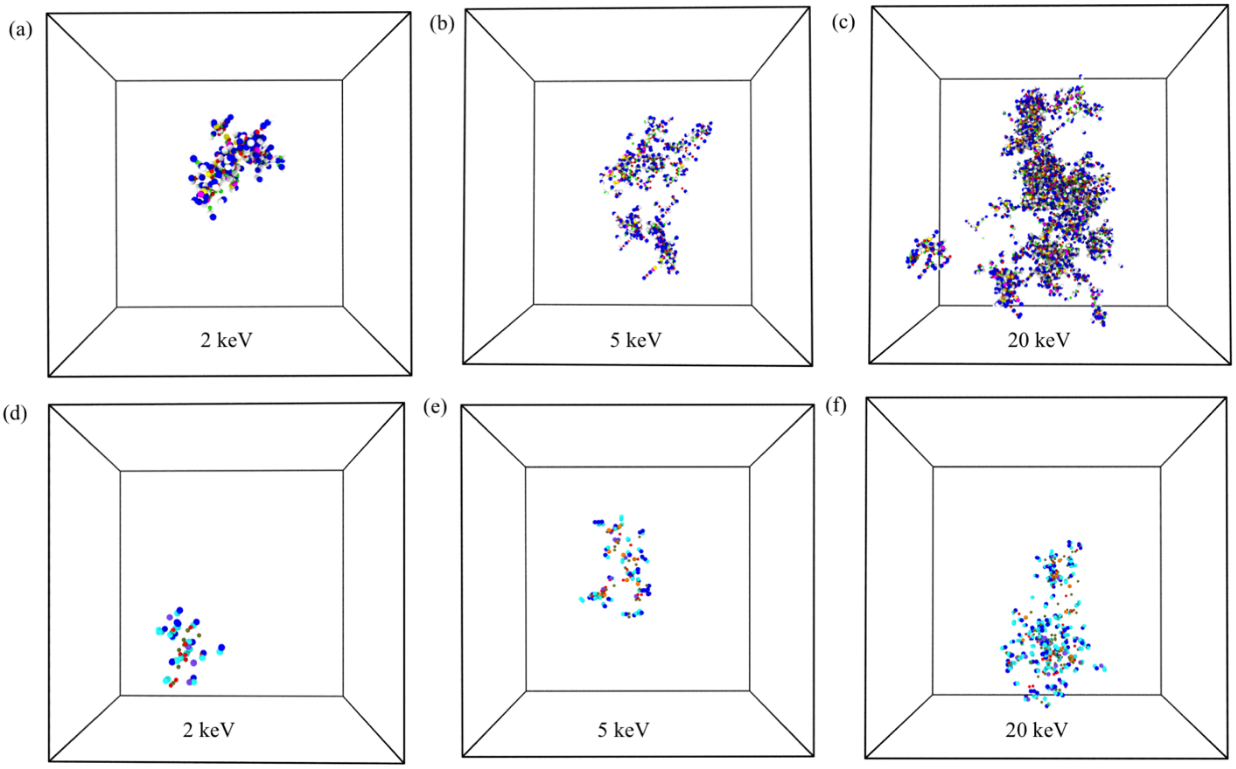

Figure 3. The Final Damage States of a 2 keV (a), a 5 keV (b), a 20 keV (c) Cascade in GaAs and a 2 keV (d), a 5 keV (e), a 20 keV (f) Cascade in GaN

4.1.2. Defect Generation

The final number of defects produced in displacement cascades is an important input to theories and models of radiation-damage evolution. Therefore, it is of great interest to calculate this parameter and compare with the standard formula in determining the displacement per atom in irradiated materials, which is developed by Norgett, Robison, and Torrens (NRT) [31]

$$N_{NRT} = 0.8E_{PKA}/2E_d, \tag{8}$$

where E_{PKA} is the energy of the primary recoil atom dissipated elastically in collisions and E_d is the mean threshold displacement energy (14 eV [18] for GaAs and 50 eV for GaN [32]). Figure 4 presents the final number of Frenkel pairs, N_F, created at the final damage state as a function of PKA energy, along with the values determined by the NRT model. It is worth mentioning that the NRT model originates from a binary-collision approximation. It is not able to describe the atom interactions in later stages. As expected, the NRT model underestimated the total number of Frenkel pairs in GaAs that have been obtained from our MD simulation, since NRT has its shortage in describing the subsequent stages in collisional and thermal spike phases. Such underestimation may be due to the existence of amorphous domains. However, the total number of defects simulated in GaN can be very well predicted by the simplified NRT formula. The interstitials can easily recover to the lattice sites resulting in a small number of surviving defects.

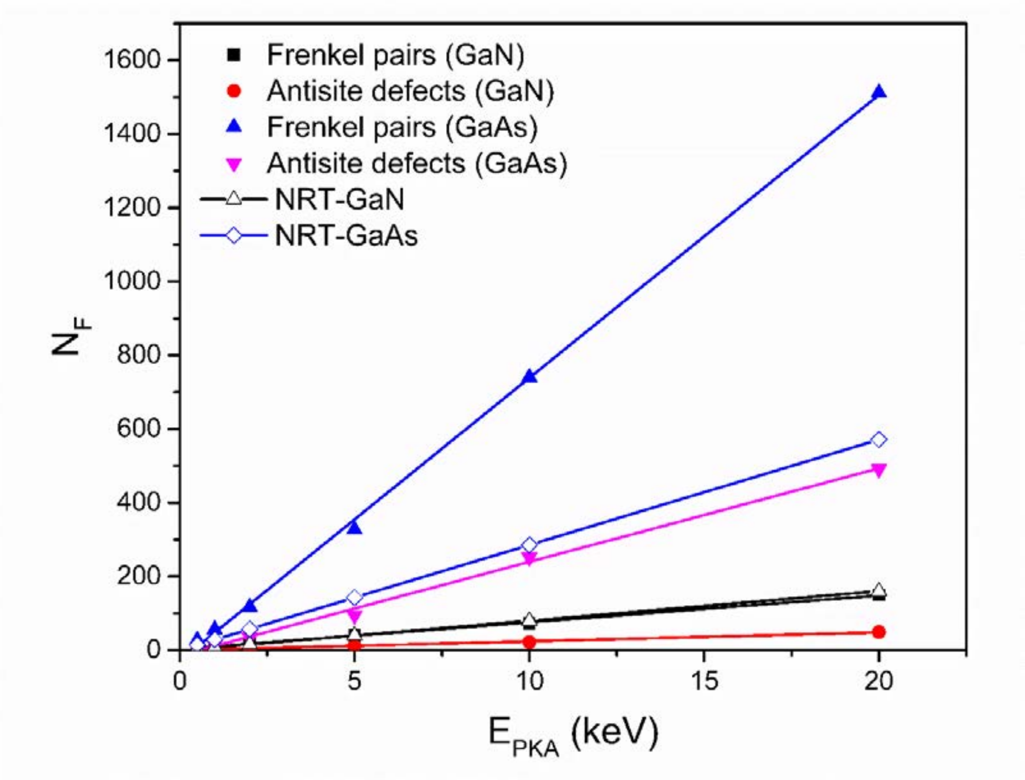

Figure 4. Number of Surviving Defects in the Cascades as a Function of PKA Energy, where Summation of Frenkel Pairs and Anti-site Defects are Presented

4.1.3. Effective NIEL

To calculate the effective NIEL, we have used the number of Frenkel pairs, ${N_F}^{MD}$, obtained from our MD simulation to extrapolate the values into the high energy regime. The energy density deposited by a PKA is equal to $\rho_{ed}=E_{PKA}/N_{pk}$ based on the assumption that energy transfer occurs just before the peak damage. Thus, the number of surviving defects can be described as

$$N_F^{MD} = A(E_{PKA})^n \rho_{ed}^m, \tag{9}$$

where A, n, and m are dimensionless parameters, which can be directly determined by fitting the MD data. Their values are summarized in Table 1.

Table 1. The Dimensionless Parameters Required to Extrapolate data into High Energy Regime

	A	n	m
GaAs	7635.95	2.15	1.11
GaN	0.05	0.95	-0.54

Based on NIEL equations detailed in [8,9] and earlier reports, the effective NIELs of GaAs and GaN are calculated for incident proton, alpha, and Xe particles with an extension of energy up to 10 MeV as illustrated in Figure 5. In general, the NIEL increases with increasing energy within a certain energy range. Beyond this range, the value decreases. The peak position and magnitude of the NIEL for both GaAs and GaN have a strong dependence on the incident particle type. Among them, proton and alpha were found to be similar in terms of the peak location. The Xe particle with larger mass leads to a higher incident energy to reach the peak value. For an incident proton particle, Khanna *et al.* [33] predicted the NIEL value in GaN using a K-P model which is an analytical approach, in which the displacement damage is proportional to the kinetic energy of recoil atoms. This prediction presents a similar tendency as our calculation. However, their value is slightly higher in magnitude than our MD-based model. This discrepancy is due to the fact that the simple NRT formula is based on the binary-collision approximation, while the number of defects created by MD simulation is often smaller than the NRT model for a given energy [34]. In addition, the NIEL has also been determined for incident protons in GaAs at high energies using the Transport of Ions in Matter (TRIM) code [35]. These data points are generally smaller than the MD modeled NIEL. The difference becomes severe when energy goes higher. This is expected since the TRIM calculation neglects the recombination process.

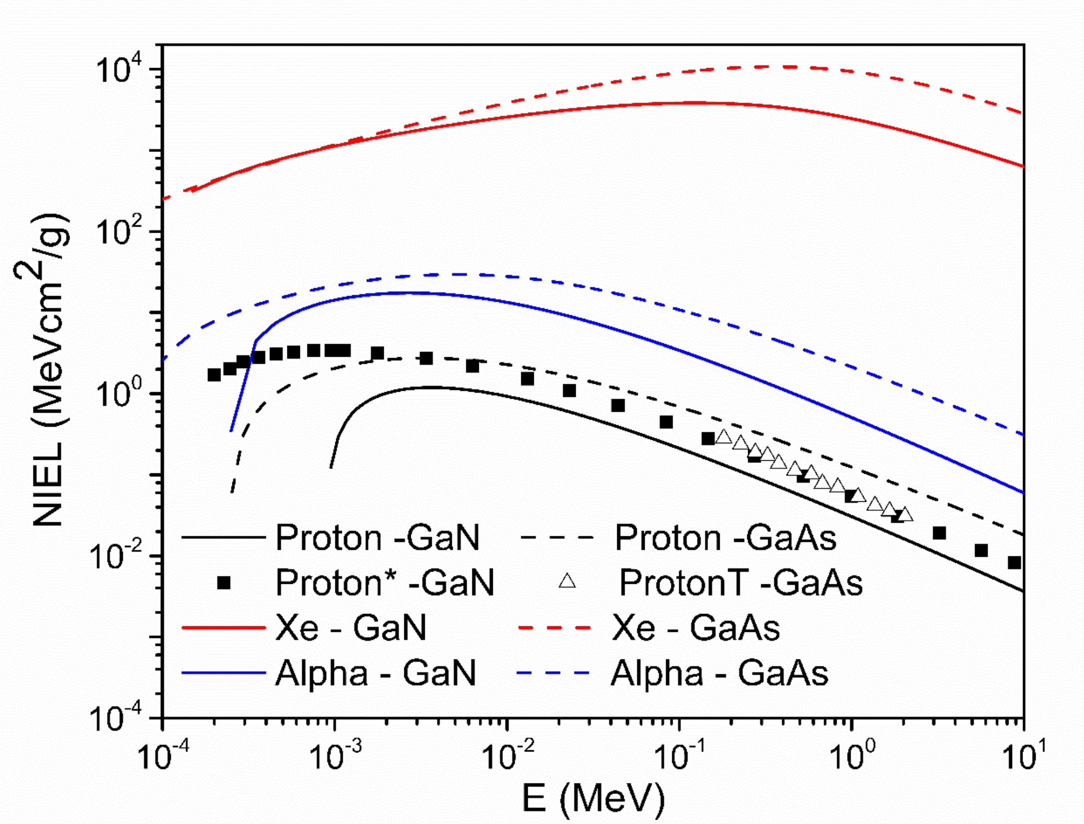

Figure 5. NIEL Calculated Based on the MD Results by a PKA for Proton, Alpha, and Xe Particle. Filled Square is from Reference [33]; Open Triangle is from Reference [35]

Meanwhile, the effective NIEL in GaN is always smaller than that in GaAs. To obtain an intuitive image of the difference between GaAs and GaN in NIEL. We have also calculated the MD NIEL ratio for GaAs-to-GaN irradiated by proton, alpha, and Xe particle, respectively. The lowest ratio for proton particle is found to be 2.30 at 3.95 keV, while the lowest value for alpha particle is 1.49 at 1.15 keV. When a heavy ion Xe is incident at a certain low energy, i.e. 350 eV, the NIELs of GaAs and GaN are almost identical with the ratio being 1.01.

4.2. AB Inito Calculations of Defects in InAs

4.2.1. Defect Formation Energy

To reduce the artificial self-image interactions imposed by periodic boundary conditions, the defects are in general modeled in a large super cell. The selection of the supercell size is a compromise of the accuracy and the computing demands. In general, the defect formation energy for a defect with charges in a semiconductor or insulator has contributions from both ions and electrons. In a supercell formalism, for a defect or impurity X in charge state q, the formation energy of this defect E f (X q) is computed by

$$E^{f}(X^{q},E_{F}) = E^{tot}(X^{q}) - E^{tot}\ (q=0) - \Sigma_{i}\Delta n_{i}\nu_{i} + q(E_{VBM} + E_{F}\ ) + E^{corr}, \qquad (10)$$

where E_{tot} (X^q) is the total energy of the supercell containing the defect X in charge state q, E_{tot} (q = 0) is the total energy of the pristine bulk supercell which is neutral and free of any defects, Δni is the number of atoms of species i added to (Δni>0) or removed from ($\Delta n_i<0$) the supercell as a result of forming the defect, $\nu_i = \nu_{bulk} + \Delta\nu_i$ is the chemical potential of element species i. When an atom is added to the system, the associated electrons are also added to the system and contribute to the formation energy. Such contribution is in form of the chemical potential of electrons, which is also known as the Fermi level E_F. The Fermi level of a semiconductor is treated as an independent variable that can assume any value within the bandgap. It is worth noting that this Fermi level is referred to as E_{VBM}, energy of valence band maximum (VBM) of the bulk material.

Since the exact value of the chemical potential cannot be determined, it is used as a parameter for the formation energy calculations. As such, the defect formation energies are given in the limiting conditions of As-rich and In-rich growth regimes. In the As-rich regime, the chemical potential of As is assumed to be its chemical potential in bulk As, whereas in the In-rich (As-poor) regime, it corresponds to the chemical potential difference between InAs and bulk In (and vice versa for the chemical potential of In). For an in-depth discussion of formation energy calculations, the reader is referred to the following papers [36-39].

The correction term of Ecorr is used to remove the errors introduced by finite size effects and the periodic boundary conditions, such as spurious overlaps of neighboring defect wave functions and, in case of charged defects, Coulomb interactions between image charges. There are still extensive debates on the performance and applicability of different schemes of corrections [40-42], for example Makov and Payne (MP) scheme [43], alignment-only scheme [44], Freysoldt, Neugebauer and Van de Walle (FNV) scheme [45], Lany and Zunger (LZ) scheme [46]. The mutual relation between the various schemes and in defining the conditions for their applications are discussed by Komsa *et al*. [47]. The classical MP scheme gives the correction terms as:

$$\mathrm{E}^{\mathrm{corr}}(q,L) = E_{mono}^{corr} + E_{quad}^{corr} = -\frac{\alpha q^2}{\epsilon L} + \frac{A_3}{L^3} \qquad (11)$$

The first term is the monopole Madelung term [41], and the second term is the third-order quadrupole electrostatic correction. The constant α is the Madelung constant of the crystal, q is the defect charge state, embedded in a uniform compensating background charge, with the unit of e, the positive electron charge. ε is the static dielectric constant. The third-order parameter A3 is a fitting parameter.

Some studies showed that the quadrupole correction does not always improve results, leaving its utility somewhat in question [48, 49]. Therefore, we only consider the leading term of the monopole Madelung correction. The Madelung constant α is 1.638 for zinc blende cubic lattice of point charges, and 2.8373 for simple cubic lattice of point charges. Within the approximation of the single charge monopole, we adopt α = 2.8373 for the cubic system. ε = 15.15 is the static dielectric constant of InAs.

4.2.2. Atomistic Defect Structures

Under the ambient condition, the InAs, one of the most important III-V semiconductor has the crystalline structures of cubic 3C zinc-blende (*zb*) structure, We firstly have optimized the geometry of the pristine *zb*-InAs with lattice parameters measured between 6.0584 Å and 6.060 Å [50]. Our result of the lattice parameter of 6.058 Å from GGA-PBEsol agrees well with previous GGA-PBE results of 6.059 Å [50], PBE-PW91 results of 6.061 Å [51], and experiment of 6.0588 Å reported by Thompson, Rowe, and Bubenstein in 1969 [52].

Then we generate 15 defect configurations with intrinsic point defects of *zb*-InAs as depicted in Figure 6. Each defective configuration sits around the center of a 3 × 3 × 3 supercell with 216 lattice sites, which ensures the interactions between images are sufficiently small. All these defect configurations are fully relaxed so that the maximum amplitude of the forces on every atom is less than 0.02 eV/Å. The final relaxed atomic structures of these 15 configurations at neutral state (charge q = 0) are displayed in Figure 6. To denote these point defects, we take the form of the element or vacancy (V) with the subscript of the site. For example, As_{110} means a configuration that has an As atom on the <110> dumbbell position, and InAs means a configuration that in which an In atom replaces an As atom on site.

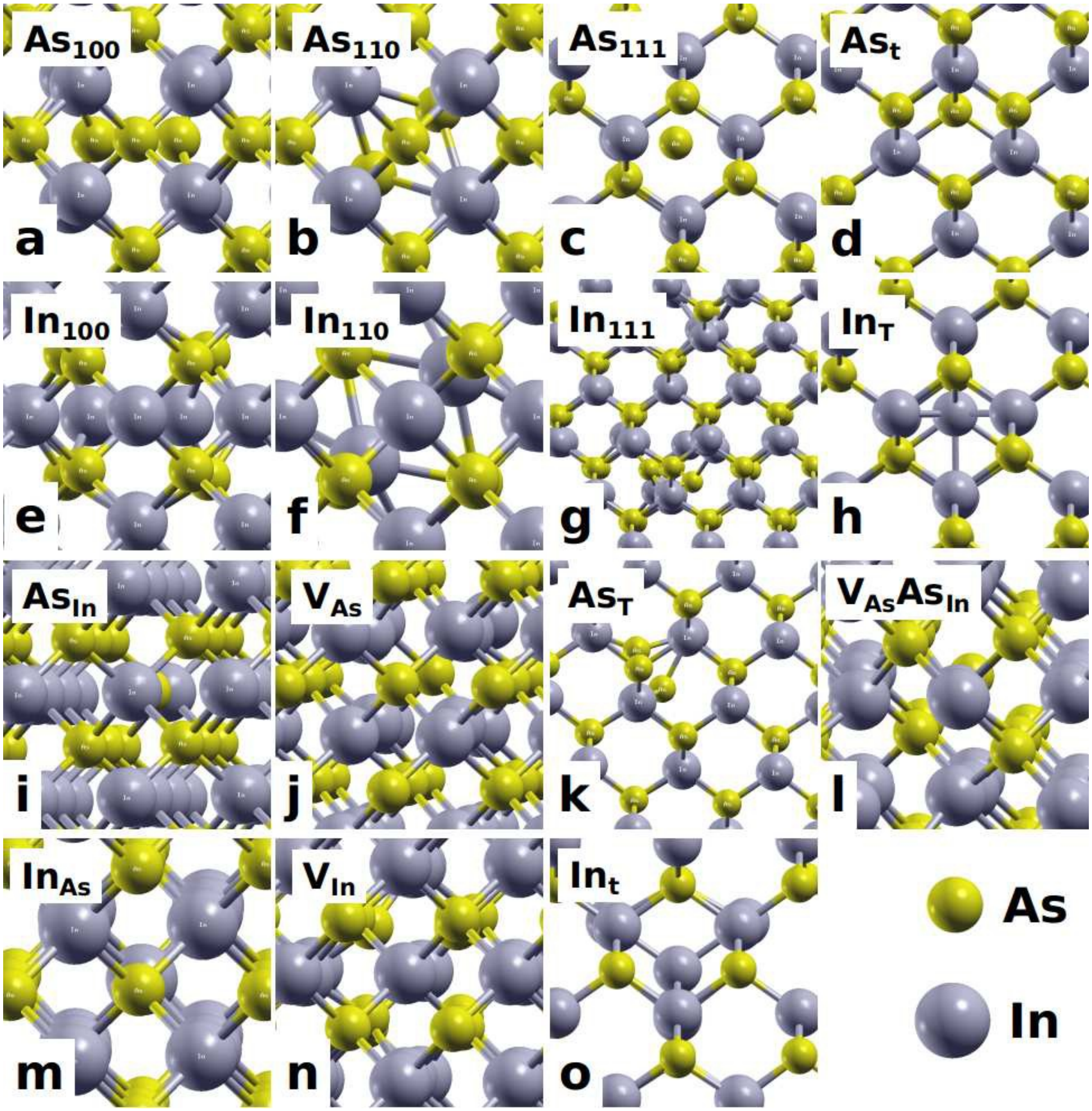

Figure 6. 15 Defect Configurations: (a) As_{100}, (b) As_{110}, (c) As_{111}, (d) As_t , (e) In_{100}, (f) In_{110}, (g) In_{111}, (h) In_T , (i) As_{In}, (j) V_{As}, (k) As_T , (l) $V_{As}As_{In}$, (m) In_{As}, (n) V_{In}, (o) In_t.

These defects are divided into five groups. The first group is the dumbbell interstitial- type point defects. The dumbbell configuration is formed when two atoms of the same species share one lattice site. There are three typical orientations as < 100 >, < 110 >, and < 111 >. Therefore, there are six dumbbell configurations: (a) As_{100}, (b) As_{110}, (c) As_{111}, and (e) In_{100}, (f) In_{110}, (g) In_{111} shown in Figure 6. The second group is the tetrahedral interstitial-type point defects. There are two kinds of tetrahedral sites in a *zb*-InAs lattice: one is formed by four In atoms denoted as “t” site, and the other is formed by four As atoms denoted as “T” site. Both In and As atoms could take either site, resulting in four tetrahedral interstitial-type point defects: (d) As_t , (h) In_T , (k) As_T, and (o) In_t shown in Figure 6. The third group is the substitutional point defects, where a pristine As site is replaced by an In atom, or vise versa. The two intrinsic substitutional point defects in *zb*-InAs are (i) As_{In} and (m) In_{As} shown in Figure 6. The fourth group is the vacancy-type point defects. There are two kinds of intrinsic vacancy-type point defects in *zb*-InAs, as (j) V_{As} and (n) V_{In}, shown in Figure 6. The last group is a point-defect complex such as $V_{As}As_{In}$, which is formed by an As vacancy V_{As} combined with a substitutional As on In site (As_{In}) in the nearest neighbor site, as shown in Figure 6 (o). This defect is interesting because the In vacancy V_{In} could attract a nearby As atom to fill up, resulting in the $V_{As}As_{In}$ complex. It is worth mentioning that the relaxed atomic structure from dumbbell interstitial-type defect of In_{111} and tetrahedral interstitial-type defect of As_T are also point-defect complexes, indicating they are highly unstable. Next, we investigate the formation energies of all these defects.

4.2.3. Formation Energies

The formation energies of the defects are computed according to the Equation 3 for different charge states from $q = -4$ to $q = 4$. In order to estimate the uncertainties caused by the finite size of supercells and the spurious image interactions, we evaluated the corrections, as detailed in the method section. We found deviations of up to 0.01 eV for defects of charge of $q = \pm 4$. We regard these values as unavoidable uncertainties that nevertheless do not alter significantly the main conclusions.

It is clear from the formation energy formula of Equation 3 that the formation energies of intrinsic defects depend on the choice of chemical potentials, i.e., the choice of reservoir with which equilibrium is achieved. The chemical potentials are constrained by equilibrium conditions, which vary from case to case, location to location, time to time. Here we only consider two extreme conditions as (1) As-rich and (2) In-rich.

Another factor we need to consider is the Fermi level, which is required for counting the formation energies from the electrons' contributions. However, the exact value of the Fermi level is also very sensitive to the local environment including doping concentrations. As a result, we have expressed the defect formation energy as a function of the Fermi level which varies in the whole range of the electronic band gap. The experimental value of the bandgap is 0.418 eV. We adopted this value as the Fermi level range in this study.

The formation energies of the 15 defect configurations in the dilute limit are computed using the supercell method as aforementioned. The formation energies as a function of the Fermi level in the As-rich environment and In-rich for all these intrinsic defects of zb-InAs with all possible charge states from -4 to +4 are displayed in left and right panels of Figure 7, respectively. Our results show the distinctive trend and large variations of the formation energies under various charge states as a function of Fermi level for each point defect for both As-rich and In-rich environments. All the possible formation energies are larger than 1.0 eV and smaller than 9.0 eV. The general trend is that the formation energy decreases for negative charge states ($q < 0$) and increases for positive charge states ($q > 0$) when the Fermi level increases. The slope of the formation energy as a function of Fermi level is positively correlated with the charge state. For $q = +4e$, the amount of the increment in the formation energy is larger than 1.5 eV when the Fermi level changed from VBM (0 eV) to CBM (0.418 eV).

The defect formation energy is the minimum energy for the generation of that defect. It is more practical to analyze the minimum formation energies among all the possible charge states given the fact that the electrons have much higher motilities (over three orders of magnitude) than atoms. Therefore, we define the lowest formation energy of a defect as the minimum formation energy among all possible charge states, here $-4 < q < 4$. We focus on the discussion of the lowest formation energies of these defects among various charge states in the following subsections. For simplicity, the formation energy refers to the lowest formation energy among various charge states hereafter until specified. We will discuss the formation energies of the five defect groups in the following subsections.

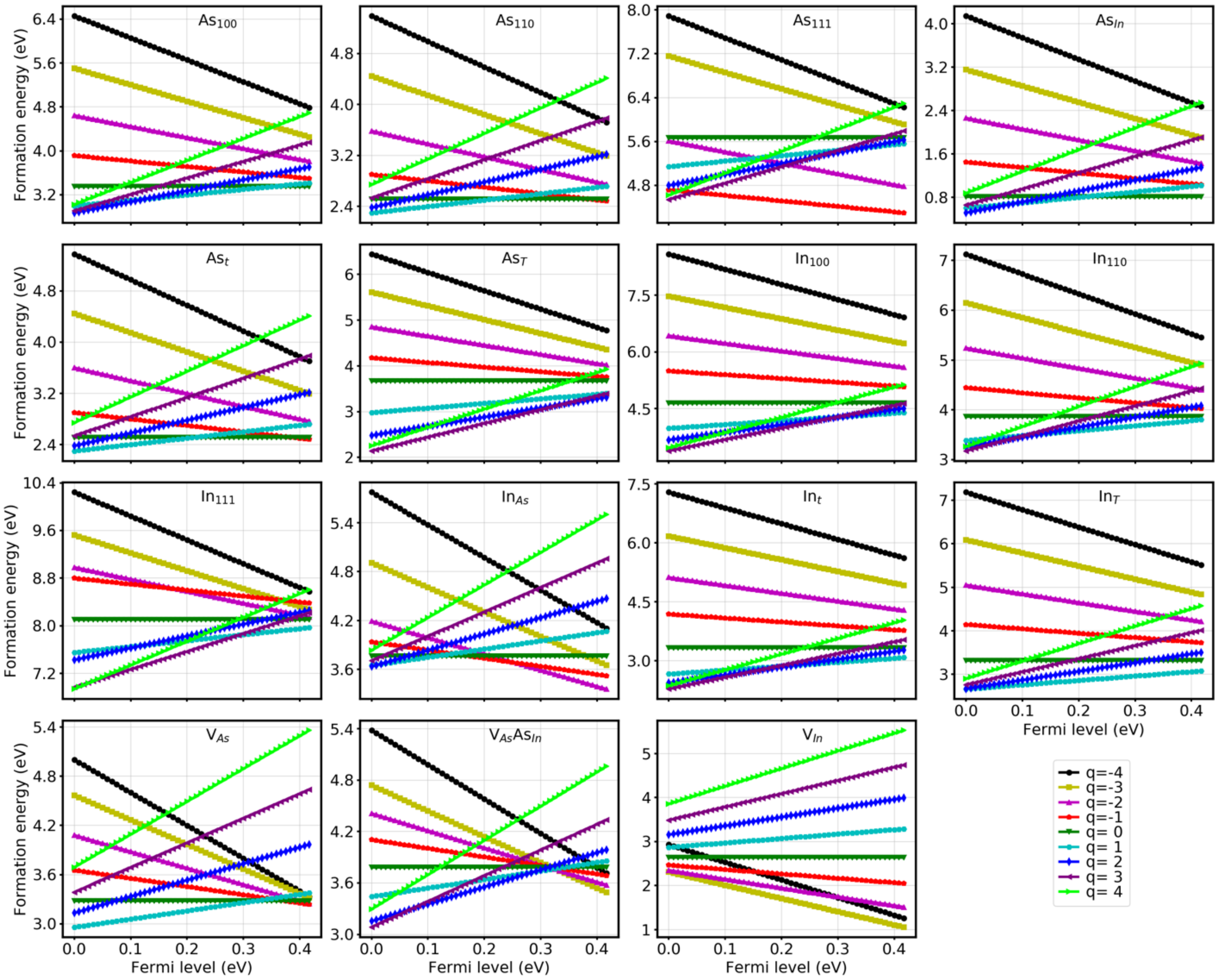

Figure 7. Formation Energy as a Function of the Fermi level at the As-rich Environment (up) and In-rich (down) for 15 type of Point defects in Zinc-blende InAs

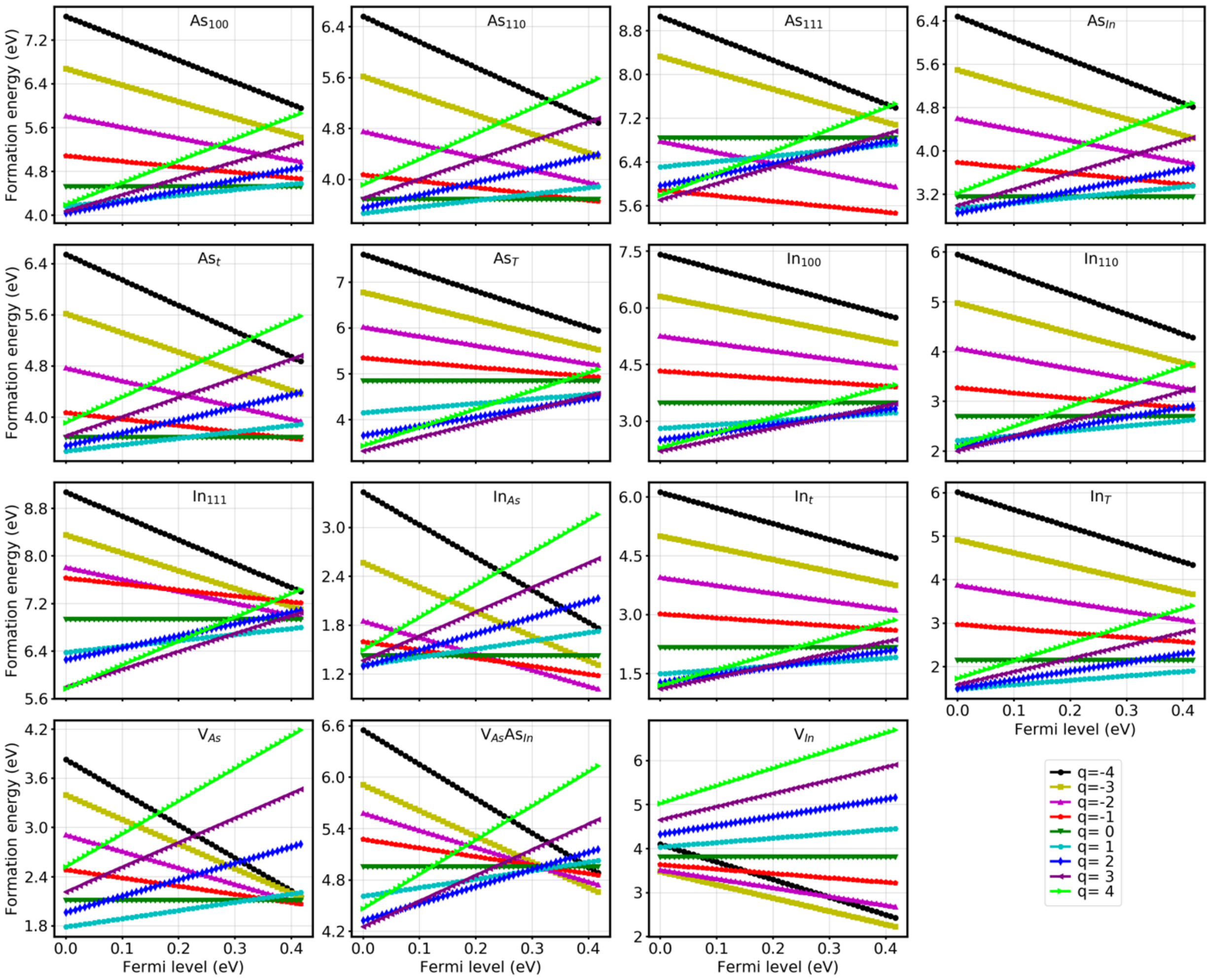

Figure 7. Formation Energy as a Function of the Fermi Level at the As-rich Environment (up) and In-rich (down) for 15 type of Point Defects in zinc-blende InAs (Continued)

4.2.4. Formation Energies of Dumbbell Interstitials

When one atom is squeezed into a lattice site taken by the same species in the pristine configuration, in general it will form a dumbbell interstitial-type point defect. We explicitly examined the six dumbbell interstitials of As$_{100}$, As$_{110}$, As$_{111}$, In$_{100}$, In$_{110}$, In$_{111}$ depicted in Figure 6. The configuration of In$_{111}$ after relaxation is much different from the original <111> dumbbell structure (not shown here but similar to Figure 6(c) for As$_{111}$ with species switched). The result indicates that In$_{111}$ is unstable and will relax to a complex simultaneously. The formation energy of these six dumbbell interstitials as a function of the Fermi level under As-rich and In-rich chemical environments are shown in the left and right panels, respectively, in Figure 8. The In$_{111}$ and As$_{111}$ have the two highest formation energies for both cases, indicating that for either environment, the <111> dumbbell configurations are unfavorable, for both In and As atoms.

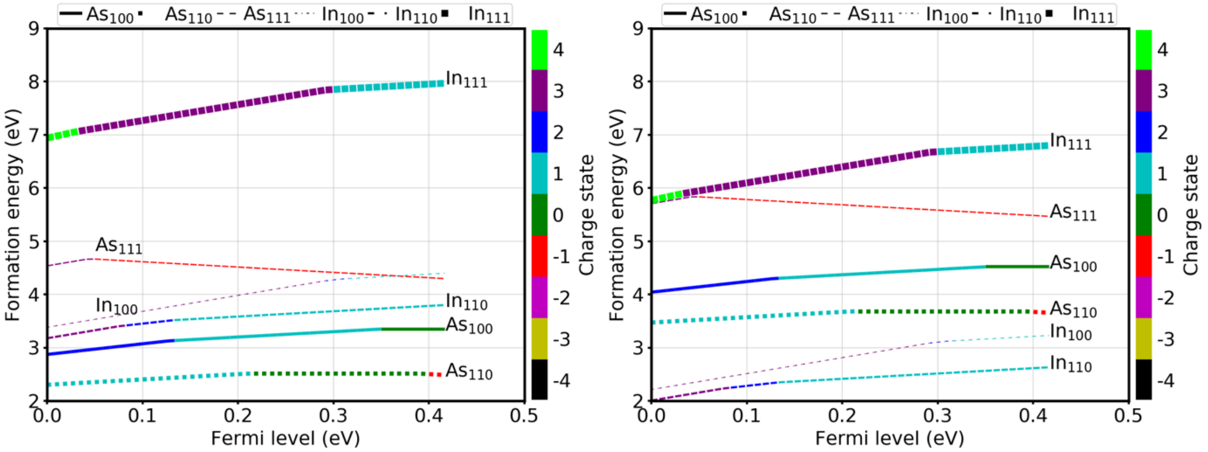

Figure 8. Formation Energy as a Function of the Fermi Level in the As-rich Environment for 6 Dumbbell Type Point Defects in zinc-blende InAs with all Possible Charge States

For an As-rich environment, the As$_{110}$ has the lowest energy among the six dumbbell interstitials, followed by As$_{100}$ and In$_{110}$. For an In-rich environment, the configurations with the lowest three formation energies are In$_{110}$, In$_{100}$ and As$_{110}$, similar to the As-rich case with switched elements. Therefore, we can conclude that the dumbbell interstitials prefer <110> configurations in *zb*-InAs under various charge states, chemical environment, and Fermi levels.

4.2.5. Formation Energies of Tetrahedral Interstitials

The tetrahedral sites are among the most energetic favorable sites for interstitials in diamond and zinc-blende structures. The four intrinsic tetrahedral interstitials of (1) As on 4-As formed tetrahedral site As$_t$, (2) As on 4-In formed tetrahedral site As$_T$, (3) In on 4-As formed tetrahedral site In$_t$, (4) In on 4-In formed tetrahedral site In$_T$ are explicitly studied. The formation energy is illustrated in Figure 9 as a function of Fermi level for both As-rich and In-rich chemical environments. There is no clear trend for all 8 cases. For As-rich environment and shallow doping of $E_F < 0.08$ eV, the As$_T$ has the lowest formation energy for the charge state of $q = +3e$. In the higher Fermi level, As$_t$, in the 4-As tetrahedral site has much lower energy than other tetrahedral configurations. The As$_T$ is energetically unfavorable at Fermi level larger than 0.26 eV. The In$_T$ prefers the $q = +1e$ in the entire Fermi level range.

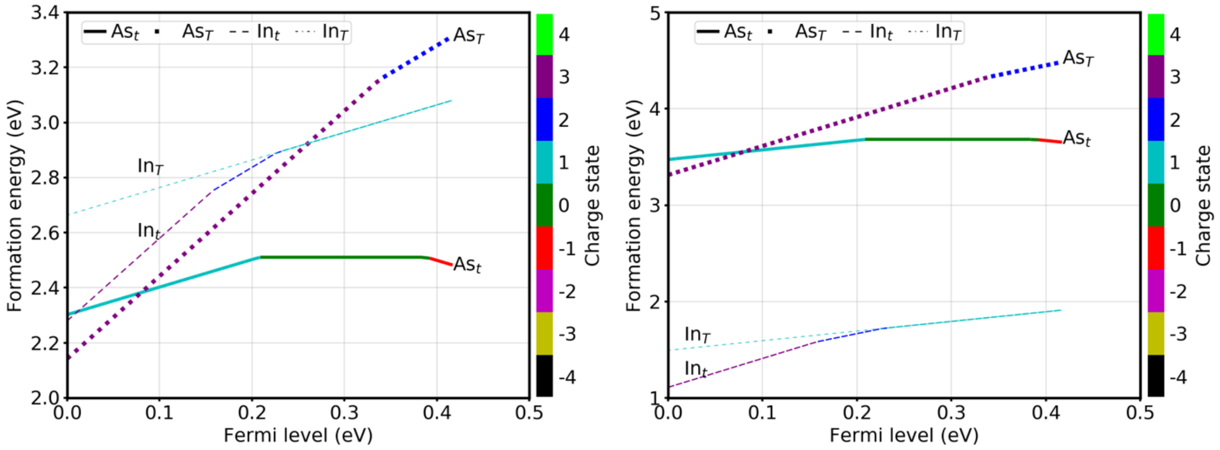

Figure 9. Formation Energy as a Function of the Fermi level in the As-rich (left) and In-rich (right) Environments for 4 tetrahedral-site Interstitial Type Point Defects

The most interesting feature of the formation energy of tetrahedra interstitials is that for both As-rich and In-rich environments, In atoms prefer 4-As tetrahedral sites until $E_F > 0.23$ eV, where In atoms have the same formation energy at both tetrahedral site with the same charge state. The identical formation energies and the charge states suggest a fast diffusion along the path of $t - T - t - T$ among the tetrahedral sites for In atoms. In addition, under an In-rich environment, the formation energies of tetrahedral interstitials of In atoms are very low, less than 2 eV. In the shallow doping case, the Int has a small formation energy close to 1 eV, with charge state of q = +3e. The low defect formation energy implies that the concentration of the corresponding defects is high at thermal equilibrium. Therefore, in the In-rich environment, the In atoms prefer tetrahedral sites with fast diffusion along the $t - T - t$ path. The quantities of diffusion behavior including diffusion energy barrier and diffusion coefficients deserve further study.

Under the In-rich environment, the formation energy of both As_T and As_t are much higher (about 2 eV) than the In counterparts, suggesting that the As tetrahedral interstitials are energetically unlikely to form. As a contrast, under the As-rich environment, all the formation energies of As and In interstitials are close to each other. As-type tetrahedral interstitials are preferred with lower formation energies.

4.2.6. Formation Energies of Substitutions

Next, we consider the substitutional intrinsic point defects. Because there are only two elements in the pristine *zb*-InAs, there are only two substitutional intrinsic point defects, as As_{In}, and In_{As}. The formation energies of both substitutions as a function of Fermi level are displayed in Figure 10 for both As-rich and In-rich chemical environments. The formation energy of substitutions is greatly affected by the chemical environment. Under As-rich environment, the As_{In} has a very low formation energy, even lower than 1 eV, which is about 3 eV lower than that of In_{As}. This result indicates that the As atoms tend to replace In atoms at In lattice sites. The concentration of As will be very high, about 54 orders of magnitude higher than that of In substitutions. In addition, As substitutions favor neutral or lower positively charged states (q = 0, +1, +2e).

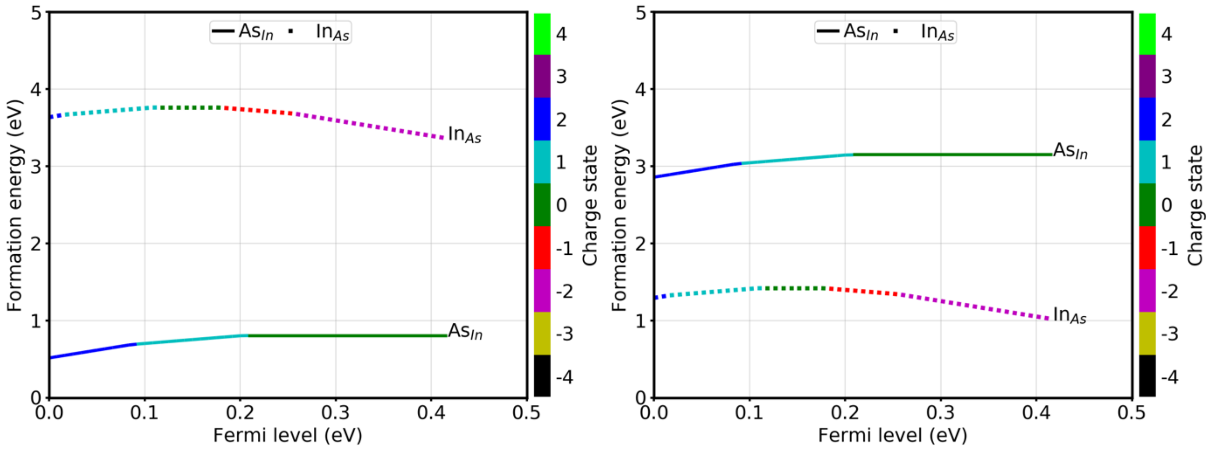

Figure 10. Formation Energy as a Function of the Fermi level at the As-rich (left) and In-rich (right) Environment for two Substitutional Type Point Defects

For In-rich environment, the In substitutions are energetically favored, with formation energy slightly higher than 1 eV, which is over 1.5 eV less than that of As substitutions. The difference in formation energy between the substitutions are less than that in the As-rich environment, implying that the difference in concentration is much less than that in the As-rich environment.

4.2.7. Formation Energies of Vacancies

The vacancy-type defects are listed among the most common defects and play an important role in vacancy-mediated diffusion and mass transport. There are two intrinsic vacancy-type point defects in InAs, as V_{As} and V_{In}. We also consider a point defect complex of $V_{As}As_{In}$. This complex is of interest because it is closely related the VIn. When one vacancy is generated on an In atom site, one As atom on nearest-neighbor site might dissociate from the host and fill the vacancy site, forming the $V_{As}As_{In}$. We have not considered the As counterpart of $V_{In}In_{As}$, as a previous study already reported that the defect complex of $V_{In}In_{As}$ is unstable and spontaneously relaxes back to V_{As} single vacancy-type defect [53].

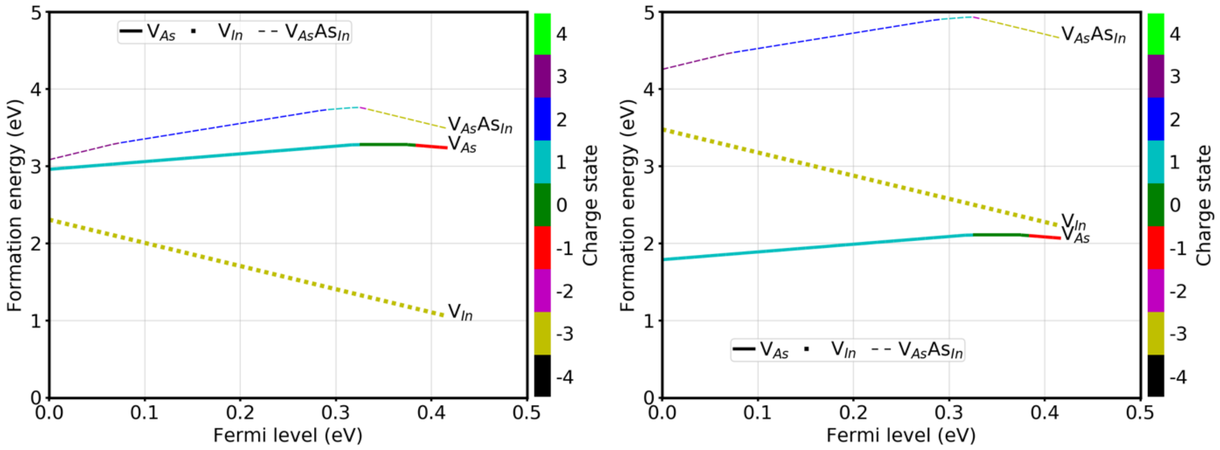

Figure 11. Formation Energy as a Function of the Fermi level at the As-rich (left) and In-rich (right) Environment for two vacancy-type Point Defects and a Point-complex

The formation energy of the three vacancy-related intrinsic defects are plotted in Figure 11 as a function of the Fermi level. For both As-rich and In-rich chemical environments, the V_{In} decreases quickly and monotonically with an increase in Fermi level. In addition, the charge state prefers $q = -3e$ throughout the whole regime. The amount of the decrease is 1.2 and 1.3 eV for As-rich and In-rich environments, respectively. Both V_{As} and $V_{As}As_{In}$ have a general trend of increasing in formation energy when Fermi level increases until $E_F > 0.33$ eV. The defect complex $V_{As}As_{In}$ has the highest formation energy among the three vacancy-related defects, larger than 3 eV, indicating that this defect complex is less favored than the single-vacancy defects.

For the As-rich environment, V_{In} has the lowest formation energy among the three kinds of vacancy-related defects. The monotonic decrease in formation energy from 2.3 eV at $E_F = 0$ to 1.05 eV at $E_F = 0.418$ indicates that the V_{In} defects are energetically favored, especially under deep doping. For the In-rich environment, the V_{As} s has the lowest formation energy, implying that the As vacancy is the dominant vacancy in In-rich *zb*-InAs.

After comparison of the formation energies within each individual defect group, it is insightful to compare all 15 intrinsic point defects globally. For that, we plotted the six lowest formation energies of the 15 defective configurations in a dilute limit as a function of Fermi level under the two extreme chemical environments of As-rich and In-rich in Figure 12.

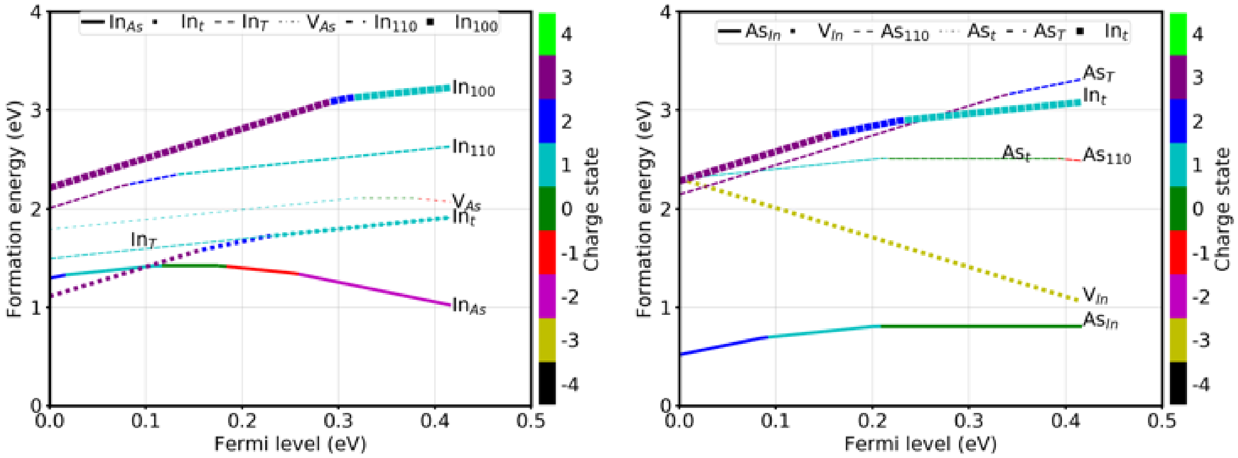

Figure 12. The six lowest Formation Energies as a Function of the Fermi level at the As-rich (left) and In-rich Environments with all Possible Charge State from -4 to +4

The chemical environment greatly changes the formation energies of intrinsic point defects. The six lowest formation energies in As-rich environments differs from that in In-rich environments for both species, amount, and charge states. For an As-rich environment, the lowest formation energy is 0.517 eV for AsIn at $E_F = 0$ eV with charge state of $q = +2e$, and 0.806 eV for $E_F > 0.21$ eV at neutral charge state. The second lowest formation energy is vacancy-type V_{In}, with formation energy as low as 1.06 eV at $E_F = 0.417$ eV. All the other point defects have formation energies larger than 2 eV, indicating much smaller concentrations than the As_{In} and V_{In} defects.

For In-rich environment, the lowest formation energies are among the In tetrahedral interstitials and substitutionals. For shallow doping Int interstitials are dominant with the lowest formation energy for $E_F < 0.1$ eV. The smallest value is 1.109 eV at $E_F = 0$ eV. The charge state is $q = -1e$. When $E_F > 0.1$ eV, the lowest formation energy among all the intrinsic point defects is substitutional In_{As}, with the minimum value of 1.019 eV at $E_F = 0.417$ eV with charge state of $q = -2e$. We can conclude that substitutional point defects are the primary intrinsic point defects in *zb*-InAs until the shallow doped In-rich environment where the dominant intrinsic point defects are In tetrahedral interstitials.

Overall, the minimum formation energy of an intrinsic point defect is predicted to be 0.517 eV in zb-InAs with AsIn configuration. It is a substitutional point defect in an As-rich chemical environment with charge state of $q = +2e$ and shallow doping regime. The predominant substitutional point defect might be useful in designing radiation tolerant electronics, as the ubiquitous point defects reduce the separation of the Frenkel pairs and enhance the recombination of the point defects under the conditions of irradiation by high energy particles. Therefore, to increase the radiation resistance, it is suggested to be in the As-rich environment.

4.3. Development of Interatomic Potentials

As reported in the 2017 report, we developed the interatomic potentials for InAs. However, we have carried out detailed calculations of defect properties using these potentials, but the results show that the defect properties cannot be well described by the potentials, as compared to the limited *ab initio* calculations. In order to obtain good potentials for InAs, which can be used to simulate displacement cascades, we reshaped our scope slightly: (a) an extensive study of defect properties using an *ab initio* approach, as described in section 4 and b) modifying the interatomic potentials based on *ab initio* results of defect properties. However, we have also used these potentials to simulate defect generation and defect clustering in InAs, but we do need more time to properly analyze the results. Therefore, the MD simulations of displacement damage and the calculations of the effective NIEL in InAs are not included in this report.

The fitting approach of an interatomic potential is similar to that described in the 2017 report. Fitting an ABOP potential requires knowledge of basic physical properties of several differently coordinated structures, such as lattice parameters, cohesive energy, and bulk modulus. However, the defect properties based on *ab initio* calculations are now included in the data base. These properties can be obtained from experimental measurements or *ab initio* calculations. In the present work, the fitting process was performed by a combination of MATLAB and Large-scale Atomic/Molecular Massively Parallel Simulator (Lammps) molecular dynamics code. The function of MATLAB is to provide the optimization tool for the potential fitting, while Lammps is used to spontaneously relax the atomic configurations of interest using a conjugate gradient algorithm, thus providing input files to generate properties so as to compare with the expected values.

The optimized values of the fitting parameters by the above method are given in Tables 2 and 3. Most of the data fitted in the current work converged well with either experiment values or *ab initio* data.

Table 2. Potential Parameters for InAs

	In-In [53]	In-As	As-As [53]
D_0 (eV)	1.5052	1.9483	7.9717
r_0 (Å)	2.6639	2.5479	1.9018
S	1.2440	1.6012	2.3439
β	1.1847	1.5291	1.2465
δ	0.0109	0.0240	0.3609
γ	4.0976	2.4639	4.8650
c	1.0853	4.7487	0.1749
d	0.9465	1.1900	0.2140
h	0.4652	0.2809	0.1261
R (Å)	3.5	3.7	3.1
D (Å)	0.1	0.1	0.1
α (Å^{-1})	1.2117	See below	2.5408

Table 3. α Parameters for Three Body Interaction

	α (Å^{-1})		α (Å^{-1})
In-In-As	-2.6694	**As-In-In**	-9.7761
In-As-In	-2.9080	**As-In-As**	8.0305
In-As-As	5.5486	**As-As-In**	15.2036

5. CONCLUSIONS

Based on the displacement damage simulated from the molecular dynamics method, the results are further analyzed and compared between GaAs and GaN, including defect production, damage morphology and defect clustering, as well as the non-ionizing energy loss (NIEL). The results demonstrate that at low energies, surviving defects are mostly single interstitials and vacancies, and only 20% of the interstitial population is contained in clusters in GaAs, but a direct-impact amorphization in GaAs occurs with a high degree of probability during the cascade lifetime for Ga PKAs (primary knock-on atoms) with energies higher than 2 keV. However, a large number of atoms will be displaced during the collisional phase with a compacted cascade volume in GaN. Consequently, a great number of displaced atoms recombine significantly with vacancies at the same time, i.e., a pseudo-metallic behavior (PMB). As a result, the majority of surviving defects are just single interstitials or vacancies for all recoil energies considered with only a small number of defects forming clusters. The total number of defects simulated in GaN can be very well predicted by the simplified Norgett, Robison and Torrens (NRT) formula due to the PMB, in contrast to GaAs where the defect number becomes much larger than the NRT value. Based on the MD results, the calculated NIEL in GaN is often smaller than that predicted by a model based on the simple Kinchin-Pease formula or SRIM calculations. The comparisons of defect creation, density and effective NIEL in GaN to those of GaAs suggest that GaN may be much more resistant to displacement damage than GaAs, and therefore, very suitable for use in high-power space-energy systems and space-probe applications.

A comprehensive study of the formation and electronic structures of 15 kinds of intrinsic point defects in InAs has been carried out using a supercell method by means of first-principles calculations within the frame of density functional theory. The 15 kinds of intrinsic point defects are in five groups, namely dumbbell interstitials, tetrahedral interstitials, substitutions, vacancies, and complexes. We have examined the formation energies of all these intrinsic point defects as a function of Fermi level in As-rich and In-rich chemical environments with charge states ranging from −4e to +4e in the dilute solution limit with finite size correction. All 15 defect formation energies are greatly influenced by the chemical environments. The substitutional point defects are the primary intrinsic point defects in *zb*-InAs until the shallow doped In-rich environment where the dominant intrinsic point defects are In tetrahedral interstitials. The <111> dumbbell interstitials are unfavorable among all the point defects. The dumbbell interstitials prefer <110> configurations. The most interesting feature of the tetrahedral interstitials is that for both As-rich and In-rich environments, In atoms prefer 4-As tetrahedral sites until $E_F>0.23$ eV, where In atoms have the same formation energy at both tetrahedral sites with the same charge state. The identical formation energies and charge states suggest a fast diffusion along the path of t−T−t among the tetrahedral sites for In atoms. The V_{In} decreases quickly and monotonically with an increase in Fermi level. In addition, the charge state prefers q = −3e throughout the whole regime. The most popular vacancy-type defect is V_{In} in an As-rich environment, but switches to V_{As} in an In-rich environment. Our results shed light on the relative stabilities of these intrinsic point defects and their relative concentrations, as well as possible diffusions. This study might be useful in defect-engineering the *zb*-InAs based semiconductors, and material design of radiation resistant electronics and sensors. In addition, the *ab initio* results will provide an extensive data base for fitting interatomic potentials for InAs.

Based on the *ab initio* calculations of defect properties, we have refitted the interatomic potentials for InAs, which play a key role to simulate defect production and clustering using the MD method. The potential parameters are fitted to the elastic moduli and structural properties using the Levenberg-Marquardt minimization algorithm with the reference data obtained from experiments and *ab initio* calculations. With an extensive database, the robust interatomic potentials for InAs have been developed. These potentials have been employed to study defect properties, defect migration, defect production, defect clustering and possible amorphization in InAs. The simulated data are being further processed and analyzed, and the results will be summarized in the near future.

REFERENCES

[1] Dyksik, M., Motyka, M., Rudno-Ruzinsk, W., Sek, G., Misiewicz, J., Pucicki, D., Kosiel, K., Sankowska, I. Kubacka-Traczyk, J., Bugajski, M., “Optical properties of active regions in terahertz quantum cascade lasers,” *Journal of Infrared, Millimeter, and Terahertz Waves,* vol **37**, no. 7, 2016, pp. 710-719.

[2] Mayer, J. W., Lau, S. S., **Electronic materials science: for integrated circuits in Si and GaAs,** New York: Macmillan; London: Collier Macmillan, 1990.

[3] Eyderman, S. and John, S., “Light-trapping and recycling for extraordinary power conversion in ultra-thin gallium-arsenide solar cells," *Scientific Reports,* vol **6**, no. 28303, 2016.

[4] Kucheyev, S., Williams, J., Jagadish, C., Zou, J., Li, G., and Titov, A., “Effect of ion species on the accumulation of ion-beam damage in GaN,” *Physical Review B,* vol **64**, no. 035202, 2001.

[5] Nord, J., Nordlund, K., and Keinonen, J., “Molecular dynamics study of damage accumulation in GaN during ion beam irradiation,” *Physical Review B,* vol **68**, no. 184104, 2003.

[6] Kim Y. S., Hummer K., and Kresse, G., “Accurate band structures and effective masses for InP, InAs, and InSb using hybrid functionals,” *Physical Review B,* vol **80**, no. 035203, 2009.

[7] Reveil M., et al., “Ab initio studies of the diffusion of intrinsic defects and silicon dopants in bulk InAs,” *Langmuir,* vol **33**, 2017, pp. 11484-11489.

[8] Gao, F., Chen, N., Hernandez-Rivera, E., Huang, D., and LeVan, P. D., “Displacement damage and predicted non-ionizing energy loss in GaAs,” *Journal of Applied Physics,* vol **121**, no. 095104, 2017.

[9] Chen, N., Rasch, E., Huang, D., Heller, E. R., and Gao, F., “Atomic-scale simulation for pseudometallic defect-generation kinetics and effective NIEL in GaN,” *IEEE Transactions on Nuclear Science,* vol **65**, no. 5, 2018, pp. 1108-1118.

[10] Hopkinson, G., Dale, C., and Marshall, P., “Proton effects in charge-coupled devices,” *IEEE Transactions on Nuclear Science,* vol **43**, no. 2, 1996, pp. 614-627.

[11] Janesick, J., Elliott, T., and Pool, F., "Radiation Damage in Scientific Charge-Coupled Devices,” *IEEE Transactions on Nuclear Science,* vol **36**, no. 1, 1989, pp. 572-578.

[12] Dale, C., Marshall, P., Cummings, B., Shamey, L., and Holland, A., “Displacement damage effects in mixed particle environments for shielded spacecraft CCDs,” *IEEE Transactions on Nuclear Science,* vol **40**, no. 6, 1993, pp. 1628-1637.

[13] Gao, F., Bacon, D., Flewitt, P., and Lewis, T., “A molecular dynamics study of temperature effects on defect production by displacement cascades in α-iron,” *Journal of Nuclear Materials,* vol **249**, no. 1, 1997, pp. 77-86.

[14] Albe, K., Nordlund, K., Nord, J., and Kuronen, A., "Modeling of compound semiconductors: Analytical bond-order potential for Ga, As, and GaAs," *Physical Review B,* vol **66**, no. 3, 2002.

[15] Nord, J., Albe, K., Erhart, P., and Nordlund, K., "Modelling of compound semiconductors: analytical bond-order potential for gallium, nitrogen and gallium nitride," *Journal of Physics: Condensed Matter,* vol **15**, no. 32, 2003, pp. 5649-5662.

[16] Biersack, J. and Ziegler, J., "Refined universal potentials in atomic collisions," *Nuclear Instruments and Methods in Physics Research,* vol **194**, no. 1-3, 1982, pp. 93-100.

[17] Lindhard, J., Nielsen, V., Schar_, M., and Thomsen, P., "Integral equations governing radiation effects," *Mat. Fys. Medd. Dan. Vid. Selsk,* vol **33**, no. 10, 1963, pp. 1-42.

[18] Chen, N., Gray, S., Hernandez-Rivera, E., Huang, D., LeVan, P. D., and Gao, F., "Computational simulation of threshold displacement energies of GaAs," *Journal of Materials Research,* vol **32**, no. 8, 2017, pp. 1555-1562.

[19] Messenger, S. R., Burke, E. A., Xapsos, M. A., Summers, G. P., Walters, R. J., Jun, I., and Jordan, T., "NIEL for heavy ions: An analytical approach," *IEEE Transactions on Nuclear Science,* vol **50**, no. 6, 2003, pp. 1919-1923.

[20] Nastasi, M., Michael, N., Mayer, J., Hirvonen, J. K., and James, M., **Ion-solid Interactions: Fundamentals and Applications**, Cambridge University Press, Cambridge, UK, 1996.

[21] Kresse, G., and Furthmuller, J., "Efficiency of ab-initio total energy calculations for metals and semiconductors using a plane-wave basis set," *Computational Materials Science,* vol **6**, no. 1, 1996, pp. 15-50.

[22] Kresse, G., and Joubert, D., "From ultrasoft pseudopotentials to the projector augmented-wave method," *Physical Review B,* vol **59**, no. 1758, 1999, pp. 1758-1775.

[23] Hohenberg, P., and Kohn, W., "Inhomogeneous Electron Gas," *Physical Review B,* vol **136**, no. 3B, 1964, pp. 864-871.

[24] Kohn, W., and Sham, L. J., "Self-Consistent Equations Including Exchange and Correlation Effects," *Physical Review,* vol **140**, no. 4A, 1965, pp. 1133-1138.

[25] Perdew, J.P., K. Burke, and Ernzerhof, M., "Generalized gradient approximation made simple," *Physical Review Letters,* vol **77**, no. 18, 1996, pp. 3865-3868.

[26] Perdew, J.P., Ruzsinszky, A., Csonka, G.I., Vydro, O.A., Scuseria, G.E., Constantin, L.A., Zhou, X.L., Burke, K., "Restoring the Density-Gradient Expansion for Exchange in Solids and Surfaces," *Physical Review Letters,* vol **100**, no. 13, 2008.

[27] Nordlund, K., Ghaly, M., Averback, R., Caturla, M., de La Rubia, T. D., and Tarus, J., "Defect production in collision cascades in elemental semiconductors and fcc metals," *Physical Review B,* vol **57**, no. 13, 1998, pp. 7556-7570.

[28] Setyawan, W., Selby, A. P., Juslin, N., Stoller, R. E., Wirth, B. D., and Kurtz, R. J., "Cascade morphology transition in bcc metals," *Journal of Physics: Condensed Matter,* vol **27**, no. 22, 2015.

[29] Gao, F. and Weber, W. J., “Atomic-scale simulation of 50 keV Si displacement cascades in β-SiC,” *Physical Review B,* vol **63**, no. 054101, 2000.

[30] Gao, F., Bylaska, E. J., Weber, W. J., and Corrales, L. R., “Native defect properties in β-SiC: Ab initio and empirical potential calculations,” *Nuclear Instruments and Methods in Physics Research Section B: Beam Interactions with Materials and Atoms,* vol **180**, no.1-4, 2001, pp. 286-292.

[31] Norgett, M. J., Robinson M. T., and Torrens I. M., “A proposed method of calculating displacement dose rates,” *Nuclear Engineering and Design,* vol **33**, no.1, 1975, pp. 50-54.

[32] Xiao, H., Gao, F., Zu, X. T., and Weber, W. J., “Threshold displacement energy in GaN: Ab initio molecular dynamics study,” *Journal of Applied Physics,* vol **105**, no. 123527, 2009.

[33] Khanna, S. M., et al., “Proton energy dependence of the light output in gallium nitride light-emitting diodes,” *IEEE Transactions on Nuclear Science,* vol **51**, no.5, 2004, pp. 2729-2735.

[34] Bacon, D. J., Calder A. F., and Gao F., “Defect production due to displacement cascades in metals as revealed by computer simulation,” *Journal of Nuclear Materials,* vol **251**, 1997, pp. 1-12.

[35] Summers, G. P., Burke, E. A., Shapiro, P., Messenger, S. R., and Walters, R. J., “Damage correlations in semiconductors exposed to gamma, electron and proton radiations,” *IEEE Transactions on Nuclear Science,* vol **40**, no. 6, 1993, pp. 1372-1379.

[36] Wang, J., Lukose, B., Thompson, M.O., Clancy, P., “Ab initio modeling of vacancies, antisites, and Si dopants in ordered InGaAs,” *Journal of Applied Physics,* vol **121**, no. 045106, 2017.

[37] Northrup, J. E., and Zhang S. B., “Dopant and defect energetics: Si in GaAs,” *Physical Review B,* vol **47**, no. 11, 1993, pp. 6791-6794.

[38] Lee, C.-W., et al., “Energetics of neutral Si dopants in InGaAs: An ab initio and semiempirical Tersoff model study,” *Physical Review B* , vol **91**, no. 9, 2015.

[39] Lee, S. G., and K.J. Chang, K. J., “Energetics and hydrogen passivation of carbon-related defects in InAs and In0.5Ga0.5A,” *Physical Review B,* vol **53**, no.15, 1996, pp. 9784-9790.

[40] Freysoldt, C., Grabowski, B., Hickel, T., Neugebaruer, J., “First-principles calculations for point defects in solids,” *Reviews of Modern Physic*, vol *s* **86**, no. 1, 2014, pp. 253-305.

[41] Leslie, M., and Gillan N. J., “The energy and elastic dipole tensor of defects in ionic crystals calculated by the supercell method,” *Journal of Physics C: Solid State Physics,* vol **18**, no. 5, 1985, pp. 973-982.

[42] Schultz, P.A., “Charged Local Defects in Extended Systems,” *Physical Review Letters,* vol **84**, no. 9, 2000, pp. 1942-1945.

[43] Makov, G., and Payne M. C., “Periodic boundary conditions in ab initio calculations,” *Physical Review B,* vol **51**, 1995, pp. 4014-4022.

[44] Van de Walle, C. G., and Neugebauer, J., “First-principles calculations for defects and impurities: Applications to III-nitrides,” *Journal of Applied Physics,* vol **95**, no. 8, 2004, pp. 3851-3879.

[45] Freysoldt, C., Neugebauer J., and Van de Walle, C. G., “Fully Ab Initio Finite-Size Corrections for Charged-Defect Supercell Calculations,” *Physical Review Letters,* vol **102**, no. 016402, 2009.

[46] Lany, S., and A. Zunger, A., “Assessment of correction methods for the band-gap problem and for finite-size effects in supercell defect calculations: Case studies for ZnO and GaAs,” *Physical Review B,* vol **78**, no. 235104, 2008.

[47] Komsa, H.P., Rantala, T. T., and Pasquarello, A., “Finite-size supercell correction schemes for charged defect calculations,” *Physical Review B,* vol **86**, no. 045112, 2012.

[48] Castleton, C.W.M., Höglund, A., and Mirbt, S., “Managing the supercell approximation for charged defects in semiconductors: Finite-size scaling, charge correction factors, the band-gap problem, and the ab initio dielectric constant,” *Physical Review B,* vol **73**, no. 035215, 2006.

[49] Taylor, S. E., and Bruneval, F., “Understanding and correcting the spurious interactions in charged supercells,” *Phys. Rev. B,* vol **84**, no. 075155, 2011.

[50] dos Santos, C. L., and Piquini, P., “Diameter dependence of mechanical, electronic, and structural properties of InAs and InP nanowires: A first-principles study,” *Physical Review B,* vol **81**, no. 075408, 2010.

[51] Shu, H., Liang, P. Wang, L. Chen, X., Lu, W., “Tailoring electronic properties of InAs nanowires by surface functionalization,” *Journal of Applied Physics,* vol **110**, no. 103713, 2011.

[52] Thompson, A.G., Rowe, J. E., and Rubenste, M., “Preparation and optical properties of InAs1-xPx alloys,” *Journal of Applied Physics,* vol **40**, no. 8, 1969, pp. 3280-3288.

[53] Hammerschmidt, T., Kratzer, P., and Scheffler, M., “Analytic many-body potential for InAs/GaAs surfaces and nanostructures: Formation energy of InAs quantum dots,” *Physical Review B,* vol **77**, no. 23, 2008.

LIST OF SYMBOLS, ABBREVIATIONS, AND ACRONYMS

ABOP	Analytical Bond-order Potential
As	Arsenic
C	Carbon
CBM	Conduction Band Minimum
DFT	Density Functional Theory
eV	Electron Volt
FNV	Freysoldt, Neugebauer and Van de Walle
Ga	Gallium
GaAs	Gallium Arsenide
GaN	Gallium Nitride
GGA	Generalized Gradient Approximation
In	Indium
InAs	Indium Arsenide
keV	kilo electron volts
K-P	Kinchin-Pease
KS-DFT	Kohn-Sham Density Functional Theory
LMMPS	Large-scale Atomic/Molecular Massively Parallel Simulator
LZ	Lany and Zunger
MD	Molecular Dynamics
MP	Makov and Payne
N	Nitrogen
NIEL	Non-ionizing Energy Loss
NRT	Norgett, Robison and Torrens
PBE	Perdew, Burke and Ernzerh

PKA	Primary Knock-on Atom
PMB	Pseudo-metallic Behavior
RCSs	Replacement Collision Sequences
Si	Silicon
SIA	Self-interstitial Atom
Si-C	Silicon-Carbon
SRIM	Stopping and Range of Ions in Matter
TRIM	Transport Range of Ions in Matter
VASP	Vienna Ab-initio Simulation Package
VBM	Valance Band Maximum

DISTRIBUTION LIST

DTIC/OCP
8725 John J. Kingman Rd, Suite
0944 Ft Belvoir, VA 22060-6218 1 cy

AFRL/RVIL
Kirtland AFB, NM 87117-5776 1 cy

Official Record Copy
AFRL/RVSU/David Cardimona 1 cy